Original Article

TIPS Trends in Pharmaceutical Sciences 2020: 6(3): 143-152.

Effect of Transition-Metal Complex Formation on Modulated Release of Methotrexate from Nano-Hydrogels

Mahsa Taheri[1], Samira Sadat Abolmaali[1,2,*], Mozhgan Abedanzadeh[1], Samaneh Mohammadi[1], Sanaz Javanmradi[1], Ali Mohammad Tamaddon[1]

[1]Center for Nanotechnology in Drug Delivery, Shiraz University of Medical Sciences, Shiraz, Iran.
[2]Department of Pharmaceutical Nanotechnology Shiraz University of Medical Sciences, Shiraz, Iran.

Abstract

Despite the extensive application of methotrexate (MTX) as a chemotherapeutic agent and an immune system suppressor, its therapeutic implementation has been limited due to its poor pharmacokinetics, saturable cellular transport, and insufficient response in some conditions. These limitations have resulted in the development of novel formulations. A pH-dependent MTX release was indicated in our previous study on polyethyleneimine nano-hydrogels; however, it exhibited a fast drug release in phosphate-buffered saline simulating physiologic pH and tonicity conditions. Thus, the current study was aimed at the synthesis of Zn(MTX)2Cl2 complex (MTX-Zn) to modulate drug loading and release under physiologic condition (pH=7.4). MTX-Zn was synthesized by the hydrothermal method and characterized by TLC, FT-IR spectroscopy, and Eriochrome Black T complexometric titration. MTX-Zn was then loaded into the nano-hydrogels and purified through ultrafiltration. The final product was evaluated by DLS, Zeta-potential, and TEM. The variations in the drug loading and release in acidic (tumor) and physiologic media were assessed through UV-Vis spectrophotometry and dialysis methods, respectively. A 5-fold enhancement was observed in the MTX solubility in the acetate buffer; while the Log D value increased from -0.66 to 0.1 upon Zn2+ complexation, reflecting an augmentation in the drug lipophilicity. The MTX-Zn loaded nano-hydrogels exhibited desirable physicochemical features like a small hydrodynamic diameter of 125.7 nm and low polydispersity (PDI = 0.14). The results indicated that, the release tests indicated that the release of MTX-Zn involves a combination of diffusion and swelling mechanisms. MTX-Zn complexation can be applied in the sustained drug release from the nano-hydrogel formulations.

Keywords: Methotrexate, Transition metal complex, Nano-hydrogel, Poly ethyleneimine, Release

1. Introduction

Methotrexate (2, 4-diamino-N10-methyl propylglutamic acid, MTX) has been extensively applied in the treatment of solid tumors, hematologic malignancies, and autoimmune diseases. This compound has been recognized for its anti-metabolite activity through dihydrofolate reductase inhibition and subsequent disturbance in DNA and RNA synthesis. MTX can also inhibit folate-dependent enzymes, causing adenosine overproduction which evokes immunosuppression (1). Conventional formulations of MTX can be found in the forms of injectable solutions and oral tablets. The therapeutic efficacy of this compound has been limited by its poor pharmacokinetics and biodistribution and insufficient clinical response (2). In this context, various delivery systems have been developed to resolve its drawbacks. Polymeric conjugates (e.g. human serum albumin, polyethylene glycol), liposomes, microspheres, dendrimers,

Corresponding Author: Samira Sadat Abolmaali, Department of Pharmaceutical Nanotechnology and Center for Nanotechnology in Drug Delivery, Shiraz University of Medical Sciences, Shiraz, Iran.
Email: s.abolmaali@gmail.com

Recieved: 01/07/2020; Accepted: 01/09/2020

and nano-hydrogels have shown promising potentials to enhance the MTX therapeutic efficiency (3). Nano-hydrogels belong to the family of nano-scale particulate substances with several promising properties like hydrophilicity, structural versatility, biocompatibility, long life in blood circulation, and the capability of actively or passively targeting the desired bio-phase such as tumor sites (4). Owing to their cross-linked structure, they have higher swelling tendency rather than dissolution in aqueous media. This property plays a crucial role in controlling their drug release profile. Some studies have reported the use of nano-hydrogels for MTX delivery. Azadi et al. prepared MTX-loaded chitosan nanogels by the ionic gelation method and successive surface-modification with polysorbate 80 to deliver it to CNS. Their nanogels showed an average size of 118 nm, superior loading capacity (53%), and a sustained release of 60% within 48h via both passive diffusion and swelling mechanisms (5). Lysozyme-pectin nanogels were also synthesized by a self-assembly mechanism for MTX delivery purposes. The loading capacity of spherical nanogels with sizes of 109 nm was 17%, with a pH-dependent drug release in acidic media (pH=5.3) (6).

A class of nano-hydrogels has been prepared through chemical crosslinking of hydrophilic polymers (7). Branched polyethyleneimine (PEI) is a cationic polyelectrolyte containing primary, secondary, and tertiary amino groups with respective ratios of 1/4, 1/2, and 1/4 and a mean pKa range of 8.5-9 (8). PEI can be employed in chelating transition metal ions (9) to immobilize the proteins and enzymes (10), anchor metal nanoparticles (11), and deliver drugs (12) and genes (13). PEI-grafted methoxy-PEG (mPEG-g-PEI) has been widely applied for reducing immunogenicity and cytotoxicity (14). Our previous work indicated several major structural features of the PEI nano-hydrogels for effective MTX delivery (15): I) its narrow size of distribution, II) effective microencapsulation of the negatively-charged MTX, III) biodegradability of the nano-hydrogel crosslinkers (16), IV) superior biocompatibility of the nano-hydrogel over non-crosslinked PEI (17), and 5) improved pharmacokinetics and therapeutic outcomes in collagen-induced arthritis in C57Bl/6 mic model compared with free MTX (18). Nonetheless, it exhibited a fast drug release rate in phosphate-buffered saline simulating the physiologic pH and tonicity conditions.

As one of the essential trace elements, zinc ion (Zn^{2+}) is involved in the formation of various proteins and enzymes (19, 20). Historically, Zn^{2+} was first added to insulin to develop a sustained-release formulation of Neutral Protamine Hagedorn (NPH) and insulin zinc crystal (Lente). In addition to sustaining insulin absorption, Zn^{2+} complexation also improves insulin performance by protecting its chains against proteolytic enzymes, hence incrementing the in vivo insulin stability (21). Several heterocyclic compounds including MTX can serve as ligands to synthesize Zn^{2+}-coordinated compounds (22). In this context, the current research is aimed at the synthesis of $Zn(MTX)_2Cl_2$ complex (MTX-Zn) to modulate MTX loading and release kinetics from the PEI nano-hydrogels.

2. Material and Methods

2.1. Materials

Polyethyleneimine 10 kDa (corresponding to Mw/Mn of 1.4) and methoxy polyethylene glycol 2 kDa (mPEG2000–COOH) were respectively supplied from Poly Sciences Inc. (Canada) and Jenkem (USA). Dithiodipropionic acid (DTDP), 1-(3-dimethylamino-propyl)-3-ethyl carbodiimide hydrochloride (EDC), N-hydroxysuccinimide (NHS), ethylenediaminetetraacetic acid (EDTA), and 3-(4,5-dimethyl-thiazol-2-yl)-2,5-diphenyl-tetrazolium bromide (MTT) were bought from Sigma-Aldrich (USA). $ZnSO_4.7H_2O$, dichloromethane (DCM), dimethyl sulfoxide (DMSO), triethylamine, and potassium bromide (KBr) were purchased from Merck (Germany). MTX powder (free base) was donated from Heumann, China.

2.2. Synthesis and characterization of Zn $(MTX)_2Cl_2$

The synthesis procedure was done by reacting MTX with $ZnCl_2$ in double distilled water. In a typical process, an aqueous solution of anhydrous zinc chloride (0.1364 g, 1 mmol) (10 ml) was dropwise added to MTX solution under stirring at 70 °C. The mixture then experienced 48 h of incu-

bation at 70 °C. The reaction medium was slowly evaporated at room temperature; after 2 weeks, the pale-yellow crystals precipitated which were then washed with distilled water followed by 48-hour drying at 40 °C. An aliquot of the product solution was run on silica gel-coated plates and compared with free MTX using hexane/ethyl acetate/methanol solvent (1:3:6 v/v).

Zn $(MTX)_2Cl_2$ (MTX-Zn) was evaluated by Fourier-transform infrared spectroscopy (FTIR) and Eriochrome Black T (ECBT) complexometric titration. For the FTIR spectroscopy analysis, the samples were mixed with KBr and compressed into discs. A sum of 20 scans were taken using a spectrophotometer (Vertex, Bruker, Germany) which were then averaged at the resolution of 4 cm^{-1} in range of 500-4000 cm^{-1}. Eriochrome Black T (ECBT) was employed to monitor the formation of MTX-Zn complex. To this end, 0.25 mg ECBT powder was added to the tubes containing 0.5 ml MTX-Zn test solution and 0.5 ml $ZnCl_2$ (14×10^{-5} mmol) control solution. A purple color emerged upon the formation of Zn^{2+} complex. Both samples were titrated by EDTA solution (10 mM) until the solution color turned into blue. The amount of Zn^{2+} reacting with MTX was determined from the amount of consumed EDTA through the below Equation:

Amount of Zn^{2+} reacted with MTX=($MZn^{2+}\times VZn^{2+}$) - (MEDTA×VEDTA)

Where MZn^{2+}, VZn^{2+}, MEDTA and VEDTA denote the molar concentrations of $ZnCl_2$, the volume of $ZnCl_2$ solution, and the molar concentration, and volume of consumed EDTA, respectively.

2.3. Solubility and distribution coefficient

Before determining the solubility of MTX-Zn in phosphate (10 mM, pH 7.4) and acetate (10 mM, pH 5.5) buffers, 2.2 mg of the product and equal amount of free drug were individually added to 500 µl of buffer under overnight stirring at 25 °C. Afterward, the supernatants were separated using a centrifuge at 5000 rpm for 10 min followed by UV spectroscopy (BioTek, USA) at 305 nm. Apparent MTX solubility was determined from the calibration curves in the corresponding buffers.

To calculate MTX distribution coefficient (LogD) upon Zn^{2+} complexation, 1.20 mg of the product or MTX (free base) were separately dissolved in a decanter containing a predetermined amount of equilibrated phosphate buffer and 1-octanol and stirred for 24 h. The buffer phase was carefully separated, and its UV absorbance was measured. The MTX concentration was measured by the calibration curve. LogD was also determined by Eq. 1:

$$logD_{\left(\frac{Oct}{PB}\right)}=\frac{\left(C_0(\mathrm{PB})-C_{eq}(\mathrm{PB})\right)\times V_{PB}}{V_{Oct}}}{C_{eq}(\mathrm{PB})} \quad \text{(Eq.1)}$$

Where C0(PB) and Ceq(PB) represent the primary and equilibrium concentrations of MTX in phosphate buffer (pH=7.4), while VPB and VOct denote the respective volumes of phosphate buffer and octanol under the equilibrium condition.

2.4. Synthesis and loading of nano-hydrogel

Micellar template-assisted technique was utilized to prepare PEI nano-hydrogels (NG) (15). In brief, a methanolic solution of the NHS-activated ester of mPEG2000-COOH was poured to the PEI solution in DCM at mPEG/PEI weight ratio of 0.5. TEA (1%) was then employed as a proton quencher. The reaction medium was stirred for 3 h. A rotational speed vacuum (RVC 2-18, Christ, Germany) was applied to concentrate the products which were then diluted in 3 ml deionized water, dialyzed (Float-A-Lyzer 6-8 kDa, Spectrum, USA) and lyophilized (Alpha 1-2 LD, Christ, Germany). Crosslinking was achieved by dropwise addition of $ZnCl_2$ solution into 30 mg PEG-g-PEI dissolved in MES buffer (100 mM, pH 5.6) at the Zn^{2+}/Nitrogen ratio=0.2 followed by 30 min stirring until the formation of polymeric micelle templates which served as a nano-reactor during the crosslinking process. Afterward, DTDP (100 mM) in DMSO, EDC (200 mM), and NHS (200 mM) were incorporated and stirred overnight stirring. The coordinated Zn^{2+} and residual reactants were removed through dialysis (Float-A-Lyzer 3.5 kDa) in HCl solution (pH=3.0) and then distilled water.

MTX (NG-MTX) or MTX-Zn (NG-MTX-Zn) loading was accomplished by adding 3 ml NG dispersion (3 mg/ml) to the tubes containing 1.8 ml MTX-Zn solution (7.7 mg/ml) or MTX (6.4 mg/

ml) and their mixing by pipetting. The mixtures were then incubated at 25 °C for 72 h under shaking conditions. Free drug separation was achieved utilizing ultrafiltration (Amicon 3 kDa, Millipore, USA) at 3000 rpm for 30 min. MTX loading efficacy (%) and loading capacity (%) were determined according to the free MTX concentration using UV-vis spectrophotometry.

2.5. Morphology, particle size, and ζ potential

Dynamic light scattering (DLS 180˚, Microtrac, Germany) method was utilized to assess the particle size in which a patented controlled reference method was applied to incorporate 180˚ heterodyne detection by determining signals of different scattered frequencies as well as the reflected unshifted frequency of the original laser (780 nm). The Doppler frequency shift spectrum was used to evaluate the multimodal and broad size distribution. The hydrodynamic diameter of NG before and after loading was measured in 20 mM phosphate buffer (pH=7). The data analysis was conducted considering the viscosity and refractive index of water at 25 °C. The ζ potentials analysis was carried out on the diluted samples using calibrated Zeta-Check (Microtrac, Germany) for oscillating zeta streaming potential. Transmission electron microscopy (TEM, Zeiss-EM10C-80 KV, Germany) was conducted to examine the solid-sphere size and morphology of MTX-Zn loaded NG which was negatively stained by a drop of 1% uranyl acetate solution at a contact time of 20 s. The samples were air-dried before imaging.

2.6. In-vitro release

MTX or MTX-Zn release from NG was explored by dialysis (6-8 KDa) of the loaded sample dispersions in distilled water (MTX:1.937 mg or MTX-Zn:2.22 mg) in 200 ml acetate buffer (10 mM, pH 5.5, NaCl 140 mM) or phosphate buffer (10 mM, pH 7.4, NaCl 140 mM) at 37 °C. To do so, 5 ml of the media was collected and replaced with the fresh buffer in different time intervals (30 min, 1, 2, 4, 6, 8, 10, 24, 48, and 72 h). The sample absorbance was measured at 305 nm. The MTX or MTX-Zn concentrations were calculated based on their corresponding calibration curves. The release data were fitted with diverse mathematical models (zero-order, first-order, and Higuchi). The drug release mechanism was further examined by fitting the first 60% drug release results with the Korsmeyer-Peppas equations (23). The model fitness (R^2), release rate (k) and exponent (n), and the lag time (t0) were calculated considering the released portion of MTX (M/M_∞) as a function of time (t) through a non-linear regression method (Eq. 2):

$$\frac{M}{M_\infty} = k\left(t - t_0\right) \qquad \text{(Eq. 2)}$$

2.7. Statistical Analysis

Prism Software version 5.0 (GraphPad, USA) was applied for statistical analysis. P values below 0.05 were considered statistically significant and the data were reported as mean ± standard deviation (SD).

3. Results and Discussion

3.1. MTX-Zn complex

The MTX-Zn complex in double distilled water was obtained by mixing MTX (ligand) and $ZnCl_2$ (molar ratio of 2:1) at 70 °C. TLC was applied to monitor the formation of the coordination complex. The retardation factor (R_f) of MTX and MTX-Zn was determined as 0.55 and 0.41, respectively, reflecting longer retention of MTX on the plate due to its complexation with $ZnCl_2$. FTIR spectroscopy was applied for further investigation of the samples (Figure 1). Redshift of υ(C=O) from 1644 cm^{-1} (for free MTX) to 1620 cm^{-1} (for MTX-Zn) was noticed, indicating the deprotonation of the MTX carboxyl group upon complexation with Zn^{2+}, which has been similarly reported in other studies (24). Moreover, the broad υ(O-H) band of MTX carboxylic acid groups was shrank upon MTX-Zn complexation. Additionally, the presence of the coordinated water in the complex can be inferred due to the emergence of the υ(H_2O) broad band in 2500-3500 cm^{-1}. The Zn^{2+} content of the MTX-Zn sample was determined by complexometric titration technique using ECBT. Upon adding 4.3 and 14.8 µl of the EDTA solution, the MTX-Zn and $ZnCl_2$ solutions reached the titration endpoint, respectively. The EDTA reacted with Zn^{2+} at a ratio of 1:1 (25), thus, it can be concluded that about 70% Zn^{2+} ions were involved in

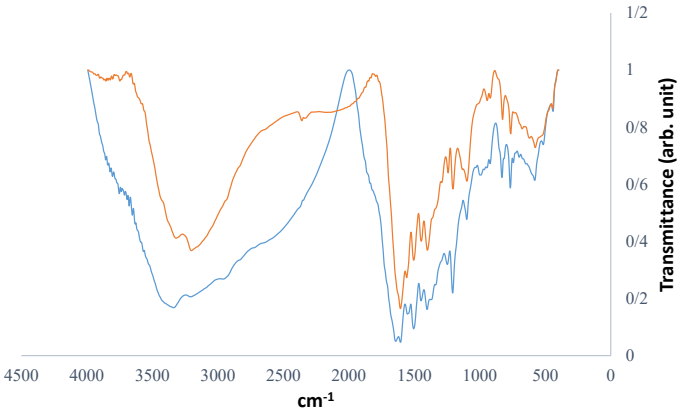

Figure 1. Comparative FT-IR spectra of MTX-Zn (orange line) vs. free MTX (blue line).

MTX-Zn synthesis.

Solubility and distribution coefficient (Log D) of the MTX-Zn sample in acetate (pH=5.5) and phosphate buffer (pH=7.4) were compared with those of MTX (free base). The solubility of free MTX was determined 2805±70 µg/ml and 205±5 µg/ml in phosphate and acetate buffer, respectively. Whereas, MTX-Zn exhibited the solubility of 1283±56 µg/ml and 1055±74 µg/ml in phosphate and acetate buffers, respectively. These results indicated and enhancement in the MTX solubility when dissolved in acetate buffer as compared with the phosphate buffer. At neutral pH, the carboxyl groups of MTX were deionized and got highly hydrated. Upon complexation with Zn (MTX-Zn), the carboxyl groups of MTX bonded with Zn^{2+}, which declined their H-bonding ability with water molecules, declining the MTX solubility (25). Furthermore, MTX-Zn enhanced the solubility of the non-ionized MTX molecules which were mainly formed in acidic media. In accordance with the solubility data, LogD values were also determined as -0.67 and +0.10 for MTX and MTX-Zn, respectively, reflecting improved lipophilicity of MTX upon complexation.

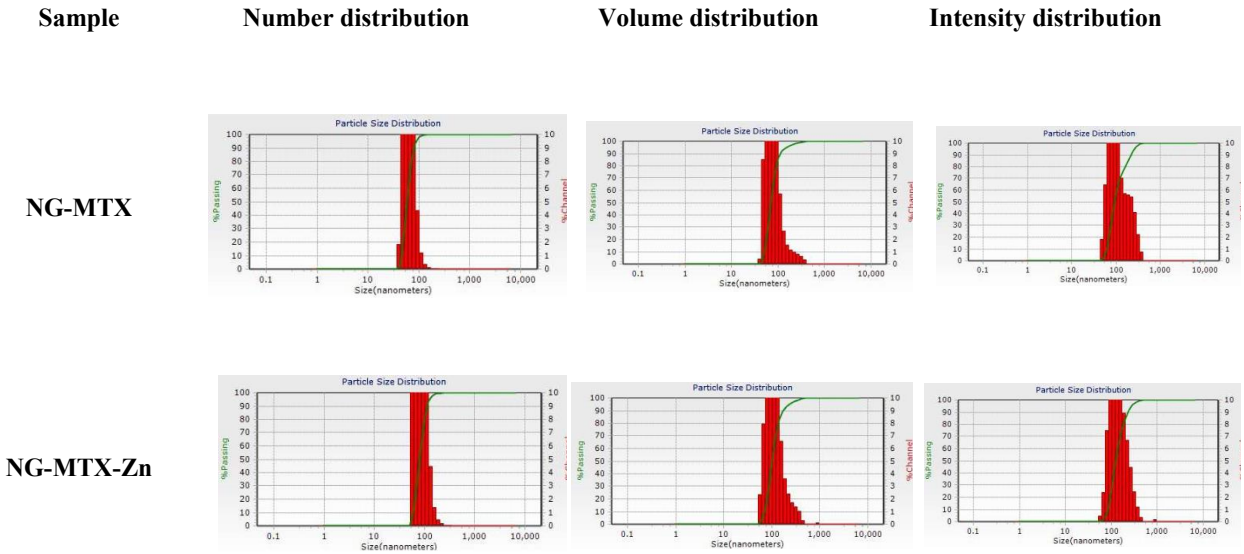

Figure 2. Hydrodynamic diameters of NG loaded with either MTX or MTX-Zn in 20 mM phosphate buffer (pH 7.4).

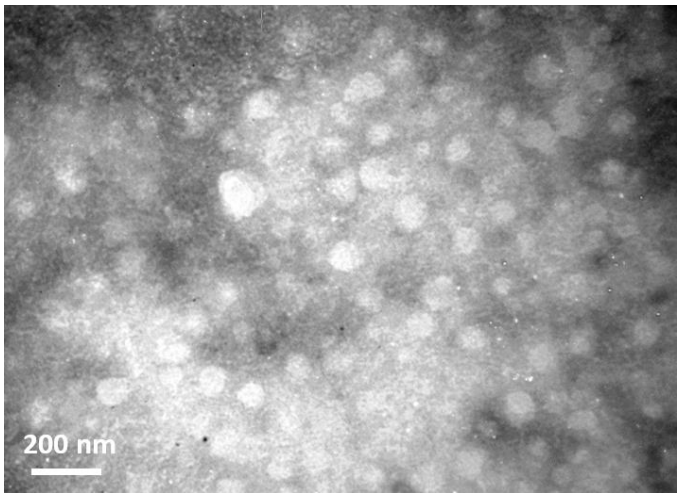

Figure 3. Transmission electron microscopy (TEM) image of the MTX-Zn loaded NG.

3.2. Morphology, particle size and ζ potential

MTX and MTX-Zn were separately loaded into NG through a post-loading process. Figure 2 depicts DLS histograms of NG, NG-MTX and NG-MTX-Zn. The mean hydrodynamic diameter of NG showed a significant decline from 366.0±21.4 nm to 92.7±9.9 and 125.7±9.5 nm in the case of NG-MTX and NG-MTX-Zn, respectively. Such a reduction in size could be assigned to the shrinkage of NG 3D-network (26, 27). Moreover, polydispersity index (PDI) decremented from 0.42±0.01 to 0.35±0.01 and 0.14±0.01 in the case of NG-MTX and NG-MTX-Zn, respectively. This descending trend can be attributed to the physical inter-chain crosslinking upon drug loading. According to Figure 2, NG-MTX-Zn particles were spherical and uniform exhibiting light grey core and dark grey boundary (Figure 3). The ζ potential of NG (+37.6±4.5 mV) declined upon free MTX or MTX-Zn loading to +6.2±1.8 and +6.4±1.5 mV, respectively. The decreased ζ potential is indicative of lower cytotoxicity of the drug loaded NGs (28). Additionally, ζ potential values in range of +/-15 mV might be regarded as a sign of particle aggregation; however, the steric hindrance of the PEG chains prevented the NGs from aggregation (15, 29).

3.3. MTX loading and in-vitro release

MTX and MTX-Zn were separately loaded into NG with the respective loading efficiency of 91.2±1.3% and 85.2±10.7%. In comparison to MTX, MTX-Zn exhibited lower (but not significant) loading efficiency. The substitution of the

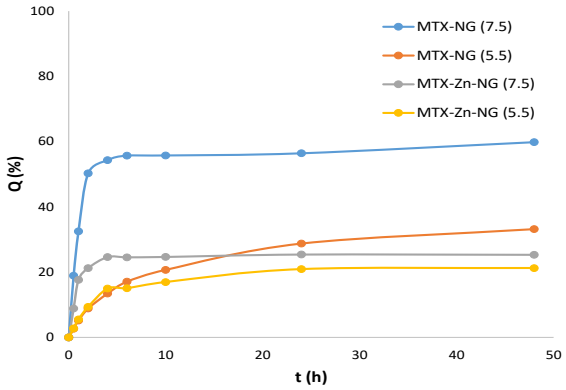

Figure 4. *In vitro* cumulative release of either MTX or MTX-Zn from NG in acetate buffered saline (pH 5.5) or phosphate buffered saline (pH 7.4) at 37 °C.

Table 1. Release kinetic parameters and statistics for the MTX-Zn loaded (NG-MTX-Zn) compared to MTX-loaded PEI nano-hydrogels (NG-MTX) in phosphate buffered saline (pH 7.4) and acetate buffered saline (pH 5.5) media

Model	Parameter / Statistic	NG-MTX (7.4)	NG-MTX (5.5)	NG-MTX-Zn (7.4)	NG-MTX-Zn (5.5)
zero order	K0 (mean)	24.49	3.27	10.38	3.67
	K0 (SE)	3.25	0.36	2.78	0.33
	R-squared	0.966	0.965	0.875	0.976
	RMSE	3.929	0.984	3.355	0.904
first order	K1 (mean)	0.77	0.40	0.66	0.41
	K1 (SE)	0.28	0.11	0.34	0.11
	R-squared	0.850	0.853	0.727	0.872
	RMSE	8.249	2.021	4.955	2.100
Higuchi	KH (mean)	35.36	6.90	15.65	7.67
	KH (SE)	3.54	0.72	2.06	0.87
	R-squared	0.980	0.969	0.967	0.963
	RMSE	2.985	0.931	1.735	1.134
Weibull	β (mean)	0.36	0.04	0.12	0.04
	β (SE)	0.02	0.01	0.03	0.01
	R-squared	0.994	0.972	0.898	0.983
	RMSE	1.641	0.880	3.034	0.773
Korsmeyer-Peppas	Kp (mean)	31.54	5.10	15.26	5.41
	n (mean)	0.68	0.71	0.53	0.74
	Kp (SE)	0.58	0.27	1.32	0.21
	n (SE)	0.03	0.05	0.15	0.03
	R-squared	0.999	0.995	0.967	0.998
	RMSE	0.728	0.370	1.728	0.291

Note: K0, K1, KH, β, Kp correspond to the rate constants in zero-order, first-order, Higuchi, Weibull and Korsmeyer-Peppas models; SE and RSME denote standard error and residual mean squared error, respectively.

H2O molecules in MTX-Zn structure with amine groups in PEI could have a decisive impact on its loading. The reported loading efficiencies were however considerably higher than the previous studies on the MTX loading into nano-hydrogels (30, 31).

Prior to the release experiment, the membrane transport of MTX-Zn was assessed under similar release conditions which exhibited a rapid drug transport through the dialysis membrane. First-order kinetic model was well fitted to the data with half-lives of 2.2 h (R2=0.99) and 3.0 h (R2=0.98) in acetate and phosphate buffer, respectively. Based on Figure 4, the MTX release was more rapid in phosphate buffer (approximately 6 times), which could be attributed to lower solubility of MTX in acetate buffer (pH=5.5) in comparison with phosphate buffer (pH=7.4) (32). Interestingly, MTX-Zn exhibited a significantly lower release rate in phosphate buffer compared with MTX. The lower solubility of MTX-Zn (see the solubility tests) and possible complexation with PEI amines of NG can explain the sustained release of MTX.

The drug release kinetics was further explored by fitting the first 60% data with Korsmeyer-Pappas model (Table 1). The mentioned model exhibited the lowest RMSE and highest R^2. As the n value lied within the range of 0.45-0.85, it can be deduced that both passive drug diffusion and NG swelling are involved in the drug release kinetics (33, 34).

4. Conclusion

MTX-Zn2+ complex was synthesized to modulate the drug release profile of the PEI nanohydrogels. Physicochemical features of drug loading at different ratios and its probable influence on the drug release and stability should be assessed prior to their safety and efficacy evaluation in cellular and animal models.

Acknowledgments

This work was a part of Ms. Taheri thesis supported financially by Shiraz University of Medical Sciences (SUMS). The facility supports of "Center for Nanotechnology in Drug Delivery" are gratefully acknowledged.

Conflict of Interest

None declared.

References

1. Koźmiński P, Halik PK, Chesori R, Gniazdowska E. Overview of Dual-Acting Drug Methotrexate in Different Neurological Diseases, Autoimmune Pathologies and Cancers. *Int J Mol Sci.* 2020 May 14;21(10):3483. doi: 10.3390/ijms21103483.
2. Yousefi G, Shafaati A, Zarghi A, Foroutan SM. Pharmacokinetics and Biodistribution of Pegylated Methotrexate after IV Administration to Mice. *Iran J Pharm Res.* 2018;17(Suppl2):111-123.
3. Abolmaali S, Tamaddon A, Dinarvand R. A review of therapeutic challenges and achievements of methotrexate delivery systems for treatment of cancer and rheumatoid arthritis. *Cancer Chemother Pharmacol.* 2013;71(5):1115-30.
4. Lombardo D, Kiselev MA, Caccamo MT. Smart Nanoparticles for Drug Delivery Application: Development of Versatile Nanocarrier Platforms in Biotechnology and Nanomedicine. *J Nanomaterials*. 2019;2019:3702518.
5. Azadi A, Hamidi M, Rouini MR. Methotrexate-loaded chitosan nanogels as 'Trojan Horses' for drug delivery to brain: preparation and in vitro/in vivo characterization. *Int J Biol Macromol.* 2013;62:523-530. doi:10.1016/j.ijbiomac.2013.10.004
6. Lin L, Xu W, Liang H, et al. Construction of pH-sensitive lysozyme/pectin nanogel for tumor methotrexate delivery. *Colloids Surf B Biointerfaces.* 2015;126:459-466. doi:10.1016/j.colsurfb.2014.12.051
7. Abolmaali SS, Tamaddon AM, Salmanpour M, Mohammadi S, Dinarvand R. Block ionomer micellar nanoparticles from double hydrophilic copolymers, classifications and promises for delivery of cancer chemotherapeutics. *Eur J Pharm Sci.* 2017;104:393-405. doi:10.1016/j.ejps.2017.04.009
8. Mintis DG, Alexiou TS, Mavrantzas VG. Effect of pH and Molecular Length on the Structure and Dynamics of Linear and Short-Chain Branched Poly(ethylene imine) in Dilute Solution: Scaling Laws from Detailed Molecular Dynamics Simulations. *J Phys Chem B.* 2020;124(28):6154-6169. doi:10.1021/acs.jpcb.0c0413
9. Chen M, Hankins NP. Interaction among branched polyethylenimine (PEI), sodium dodecyl sulfate (SDS) and metal cations during copper recovery from water using polymer-surfactant aggregates. *J Water Process Eng.* 2020;34:101170.
10. Virgen-Ortíz JJ, dos Santos JCS, Berenguer-Murcia Á, Barbosa O, Rodrigues RC, Fernandez-Lafuente R. Polyethylenimine: a very useful ionic polymer in the design of immobilized enzyme biocatalysts. *J Mater Chem B.* 2017;5(36):7461-90.
11. Li J, Yuan S, Zhu J, Van der Bruggen B. High-flux, antibacterial composite membranes via polydopamine-assisted PEI-TiO2/Ag modification for dye removal. *Chem Eng J.* 2019;373:275-84.
12. Sun X, Wang N, Yang LY, Ouyang XK, Huang F. Folic Acid and PEI Modified Mesoporous Silica for Targeted Delivery of Curcumin. *Pharmaceutics*. 2019 Aug 23;11(9):430. doi: 10.3390/pharmaceutics11090430.
13. Zhao L, Li Y, Pei D, Huang Q, Zhang H, Yang Z, et al. Glycopolymers/PEI complexes as serum-tolerant vectors for enhanced gene delivery to hepatocytes. *Carbohydr Polym*. 2019;205:167-75.
14. Safari F, Tamaddon AM, Zarghami N, Abolmali S, Akbarzadeh A. Polyelectrolyte complexes of hTERT siRNA and polyethyleneimine: Effect of degree of PEG grafting on biological and cellular activity. *Artif Cells Nanomed Biotechnol.* 2016;44(6):1561-1568. doi:10.3109/21691401.2015.1064936
15. Abolmaali SS, Tamaddon AM, Dinarvand

R. Nano-hydrogels of methoxy polyethylene glycol-grafted branched polyethyleneimine via biodegradable cross-linking of Zn2+-ionomer micelle template. *J Nanopart Res*. 2013;15(12):2134.
16. Abolmaali SS, Tamaddon A, Yousefi G, Javidnia K, Dinarvand R. Sequential optimization of methotrexate encapsulation in micellar nano-networks of polyethyleneimine ionomer containing redox-sensitive cross-links. *Int J Nanomedicine.* 2014 Jun 6;9:2833-48. doi: 10.2147/IJN.S61614. PMID: 24944513; PMCID: PMC4057327.
17. Abolmaali SS, Tamaddon AM, Mohammadi S, Amoozgar Z, Dinarvand R. Chemically crosslinked nanogels of PEGylated poly ethyleneimine (l-histidine substituted) synthesized via metal ion coordinated self-assembly for delivery of methotrexate: Cytocompatibility, cellular delivery and antitumor activity in resistant cells. *Mater Sci Eng C.* 2016;62:897-907.
18. Abolmaali S, Tamaddon A, Kamali-Sarvestani E, Ashraf M, Dinarvand R. Stealth Nanogels of Histinylated Poly Ethyleneimine for Sustained Delivery of Methotrexate in Collagen-Induced Arthritis Model. *Pharm Res.* 2015;32(10):3309-3323. doi:10.1007/s11095-015-1708-0
19. Colvin RA, Fontaine CP, Laskowski M, Thomas D. Zn2+ transporters and Zn2+ homeostasis in neurons. *Eur J Pharmacol.* 2003;479(1-3):171-185. doi:10.1016/j.ejphar.2003.08.067
20. Hou S, Vigeland LE, Zhang G, et al. Zn2+ activates large conductance Ca2+-activated K+ channel via an intracellular domain. *J Biol Chem.* 2010;285(9):6434-6442. doi:10.1074/jbc.M109.069211
21. Chance RE, Kroeff EP, Hoffmann JA, Frank BH. Chemical, physical, and biologic properties of biosynthetic human insulin. *Diabetes Care.* 1981;4(2):147-154. doi:10.2337/diacare.4.2.147
22. Zulkefeli M, Sogon T, Takeda K, Kimura E, Aoki S. Design and Synthesis of a Stable Supramolecular Trigonal Prism Formed by the Self-Assembly of a Linear Tetrakis(Zn2+−cyclen) Complex and Trianionic Trithiocyanuric Acid in Aqueous Solution and Its Complexation with DNA (Cyclen = 1,4,7,10-Tetraazacyclododecane). *Inorg Chem.* 2009;48(19):9567-78.
23. Colombo P, Bettini R, Santi P, De Ascentiis A, Peppas N. Analysis of the swelling and release mechanisms from drug delivery systems with emphasis on drug solubility and water transport. *J Control Release*. 1996;39(2-3):231-7.
24. Nodiţi G, Fulias A, Ledeti I. Methotrexate as coordination complex ligand: Study of interaction with Zn(II). *Dig J Nanomater Biostructures.* 2014;9(1):251-60.
25. Zhang Y, Li Y, Yang LQ, Ma XJ, Wang LY, Ye ZF. Characterization and adsorption mechanism of Zn2+ removal by PVA/EDTA resin in polluted water. *J Hazard Mater.* 2010;178(1-3):1046-1054. doi:10.1016/j.jhazmat.2010.02.046
26. Vinogradov SV, Kabanov AV. SYNTHESIS OF NANOGEL CARRIERS FOR DELIVERY OF ACTIVE PHOSPHORYLATED NUCLEOSIDE ANALOGUES. *Polymer Prepr*. 2004 Aug 22;228(Pt 2):296.
27. Kim JO, Sahay G, Kabanov AV, Bronich TK. Polymeric micelles with ionic cores containing biodegradable cross-links for delivery of chemotherapeutic agents. *Biomacromolecules*. 2010 Apr 12;11(4):919-26. doi: 10.1021/bm9013364. PMID: 20307096; PMCID: PMC2854228.
28. Vinogradov S, Batrakova E, Kabanov A. Poly(ethylene glycol)–polyethyleneimine NanoGel™ particles: novel drug delivery systems for antisense oligonucleotides. *Colloids Surf B.* 1999;16(1):291-304.
29. Sharma A, Garg T, Aman A, et al. Nanogel--an advanced drug delivery tool: Current and future. *Artif Cells Nanomed Biotechnol.* 2016;44(1):165-177. doi:10.3109/21691401.2014.930745
30. Lu S, Neoh KG, Huang C, Shi Z, Kang E-T. Polyacrylamide hybrid nanogels for targeted cancer chemotherapy via co-delivery of gold nanoparticles and MTX. *J Colloid Interface Sci.* 2013;412:46-55.
31. Avasatthi V, Pawar H, Dora CP, Bansod P, Gill MS, Suresh S. A novel nanogel formulation of methotrexate for topical treatment of psoriasis: optimization, in vitro and in vivo evaluation. *Pharm Dev Technol*. 2016;21(5):554-562. doi:10.3109/10837450.2015.1026605
32. Fort JJ, Mitra AK. Solubility and stability characteristics of a series of methotrexate dialkyl esters. *Int J Pharm.* 1990;59(3):271-9.
33. Barzegar-Jalali M, Adibkia K, Valizadeh H, et al. Kinetic analysis of drug release from nanoparticles. *J Pharm Pharm Sci*. 2008;11(1):167-

177. doi:10.18433/j3d59t
34. Pourtalebi Jahromi L, Mohammadi-Samani S, Heidari R, Azadi A. in vitro- and in vivo Evaluation of Methotrexate-Loaded Hydrogel Nanoparticles Intended to Treat Primary CNS Lymphoma via Intranasal Administration. *J Pharm Pharm Sci.* 2018;21(1):305-317. doi:10.18433/jpps29496